THE JOURNAL OF PHYSICAL CHEMISTRY Letters

Perspective

pubs.acs.org/JPCL

Multifaceted Excited State of $CH_3NH_3PbI_3$. Charge Separation, Recombination, and Trapping

Jeffrey A. Christians, Joseph S. Manser, and Prashant V. Kamat*

Radiation Laboratory, Departments of Chemistry & Biochemistry and Chemical & Biomolecular Engineering, University of Notre Dame, Notre Dame, Indiana 46556, United States

ABSTRACT: A need to understand the excited-state behavior of organic–inorganic hybrid perovskites, such as $CH_3NH_3PbI_3$, has arisen due to the rapid development of perovskite solar cells. The photoinduced processes leading to the efficient charge separation observed in these materials remain somewhat elusive. This Perspective presents an overview of the initial attempts to characterize the excited-state and charge recombination dynamics in the prototypical material $CH_3NH_3PbI_3$. While much has been accomplished in designing high-efficiency solar cells, the multifaceted nature of the $CH_3NH_3PbI_3$ excited state offers ample challenges for the photovoltaic community to better comprehend. Building on this foundation may enable us to tackle the stability concerns that have shadowed the rise of perovskite solar cells. Furthermore, a better understanding of the excited-state properties can provide insight into the specific properties that have thrust this material to the forefront of photovoltaic research.

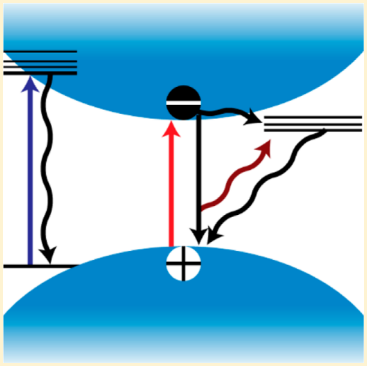

The controlled interaction between a bivalent metal halide and an organic or inorganic monovalent cation, such as methylammonium, cesium, or formamidinium, results in the formation of an ordered crystal structure analogous to that of perovskite ($CaTiO_3$). These halide perovskites, as they are known, were originally discovered in the late 1800s.[1,2] A century later, the organic–inorganic hybrid perovskites began receiving significant attention due to their interesting optoelectronic properties.[3−8] Yet, it was not until the past 5 years that the photovoltaic properties of this unique class of compounds were explored with methylammonium lead iodide, $CH_3NH_3PbI_3$, leading the way.[9,10] Despite this short development time, certified efficiencies greater than 20%[11] have amazed the scientific community and drawn in many new researchers to the field who were previously engaged in improving the performance of dye-sensitized solar cells, organic photovoltaics, and quantum dot solar cells.

> A deeper understanding of these most basic processes will be a valuable asset to researchers aiming to push the performance of perovskite solar cells nearer the Shockley–Quessier limit.

A herculean effort has, in recent years, focused on improving the photovoltaic architecture (e.g., planar versus mesoscopic) and improving photovoltaic performance, stability, and reproducibility. It is this work that has been chiefly responsible for the meteoric rise of perovskite solar cell efficiencies. On the other hand, significant gaps remain in the understanding of the excited state, charge separation, recombination, and charge trapping. However, this is not without cause. Despite a significant study into these fundamental issues, it is clear that this system presents numerous unique challenges to researchers.[12] Even so, a deeper understanding of these most basic processes will be a valuable asset to researchers aiming to push the performance of perovskite solar cells nearer the Shockley–Quessier limit and improve the stability of these devices beyond necessary commercial benchmarks.[13] Our research group has been actively involved in contributing to this growing knowledge base, probing the excited-state dynamics of $CH_3NH_3PbI_3$ and elucidating the ultrafast charge separation and charge recombination processes following short laser pulse excitation. This Perspective provides an overview of different properties of the excited state of $CH_3NH_3PbI_3$ and will hopefully provide the basis for establishing new strategies to modulate the excited-state behavior of hybrid perovskites.

Evolution of the $CH_3NH_3PbI_3$ Excited State. CH_3NH_3I (MAI) and PbI_2 can crystallize at relatively low temperatures (70–100 °C) to form $CH_3NH_3PbI_3$, which has a tetragonal perovskite structure of the general form ABX_3, where A = CH_3NH_3, B = Pb, and X = I (Figure 1). A whole host of techniques have been employed to better control $CH_3NH_3PbI_3$ film crystallinity and morphology.[14] Formation of the crystalline perovskite phase causes a color change from the yellow of the precursor solution to the dark black/brown of the $CH_3NH_3PbI_3$ with its band gap of approximately 1.6 eV.[15−17]

Because of the solution-based deposition of $CH_3NH_3PbI_3$, characterization of the complexes that form in the precursor solution offers the potential to obtain an intriguing look into

Received: March 20, 2015
Accepted: May 14, 2015
Published: May 14, 2015

DOI: 10.1021/acs.jpclett.5b00594
J. Phys. Chem. Lett. 2015, 6, 2086–2095

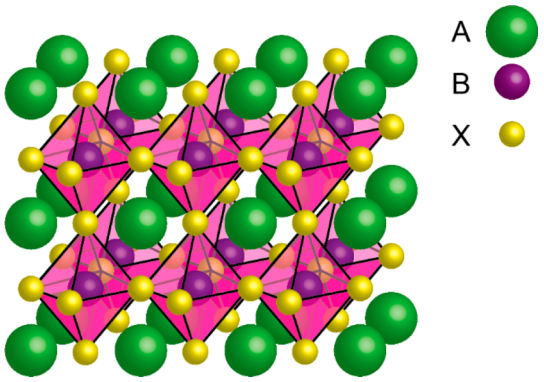

Figure 1. Scheme showing the general (ABX_3) crystal structure of perovskite. In the case of the hybrid perovskite $CH_3NH_3PbI_3$ discussed in the present Perspective, A = CH_3NH_3, B = Pb, and X = I. Reproduced with permission from ref 18. Copyright 2015, American Chemical Society.

the final perovskite.[19] Transition metals with an s^2 electron configuration (i.e., Sn^{2+}, Pb^{2+}, and others) can readily complex with halogens.[20] In solutions of PbI_2 with excess CH_3NH_3I, Pb^{2+} complexes such as triiodoplumbate (PbI_3^-, Equilibrium 1) and tetraiodoplumbate (PbI_4^{2-}, Equilibria 2) have been observed to form with equilibrium constants of K_1 = 54 M^{-1} and K_2 = 6 M^{-1}, respectively.

$$PbI_2 + I^- \overset{K_1}{\Leftrightarrow} PbI_3^- \quad (1)$$

$$PbI_3^- + I^- \overset{K_2}{\Leftrightarrow} PbI_4^{2-} \quad (2)$$

While a spectator in the precursor solutions, the organic cation becomes an integral part of the crystal structure as the lead iodide film transforms into perovskite structure upon annealing. The transformation of the lead halide complex into the perovskite structure can be readily followed through steady-state and transient absorption spectra. Distinct features of iodoplumbate complexes persist in the spectra of unannealed $CH_3NH_3PbI_3$ films (Figure 2A), red-shifted from their position in solution, red-shifting further and dampening upon annealing. This shift to lower energies is expected as solvent molecules are expelled and higher-order coordination complexes between Pb^{2+} and I^- are formed.

The evolution of the excited state shows a similar transition from the plumbate complex to crystalline $CH_3NH_3PbI_3$ (Figure 2B). Both the high energy-bleach and induced absorption peaks shift to the red upon film formation while maintaining an isosbestic point (Figure 2B, spectrum b), and a second bleach peak arises at lower energy owing to the formation of $CH_3NH_3PbI_3$ upon film drying and annealing. These peaks are then shifted further to the red as the films are annealed (Figure 2B, spectrum c) until the completely evolved spectral fingerprint of $CH_3NH_3PbI_3$ is observed. Interestingly, the prominent induced absorption peak in the excited-state spectra of the plumbate complex in solution (Figure 2B, spectrum a) correlates well with the steady-state absorption spectrum of I_2 in DMF (reaction 3).

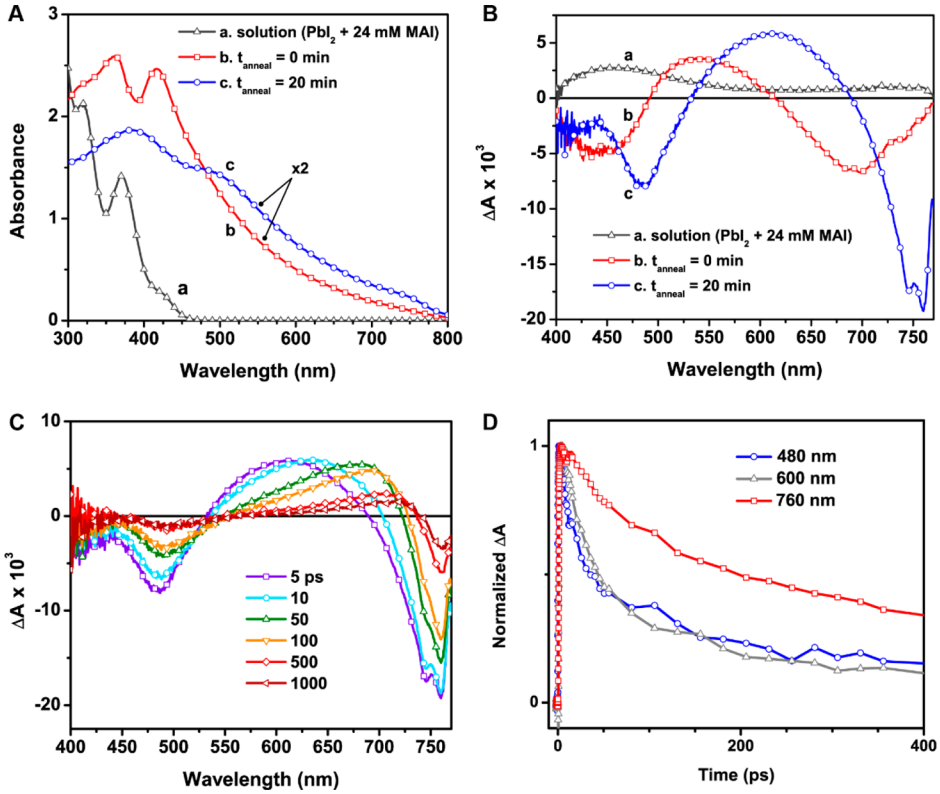

Figure 2. (A) Ground-state absorption spectra of (a) the perovskite precursor solution in DMF, (b) the as-deposited film from a 1:1 CH_3NH_3I/PbI_2 solution on alumina, and (c) after annealing the deposited film at 100 °C for 20 min. (B) Excited-state spectra of the same samples recorded 5 ps after 387 nm femtosecond laser pulse excitation in an evacuated cell. (C) Transient absorption spectra recorded following 387 nm excitation of annealed $CH_3NH_3PbI_3$ on a mesoporous alumina support at various pump–probe delay times. (D) Difference absorption–time profiles of an annealed $CH_3NH_3PbI_3$ film recorded at 480 (blue trace), 600 (gray trace), and 760 nm (red trace). Adapted from ref 21 with permission from The Royal Society of Chemistry.

DOI: 10.1021/acs.jpclett.5b00594
J. Phys. Chem. Lett. 2015, 6, 2086–2095

$$PbI_n^{(2-n)} + h\nu \rightarrow (PbI_{n-2}^{(3-n)} \cdots I_2^-) \quad (3)$$

One isosbestic point remains in the fully annealed $CH_3NH_3PbI_3$ films at 530 nm, while none exist in the 680–740 nm region of the spectrum (Figure 2C), and there exists a significant discrepancy between the excited-state recovery kinetics at 480 and 600 nm and those of the 760 nm bleach (Figure 2D).

One of the early studies explained the two transitions at 480 and 760 nm based on a dual valence band structure (Figure 3A).[22] This model predicts the accumulation of charges at a common conduction band minimum, CB1, regardless of the transition excited (viz., VB2 to CB1 or VB1 to CB1). Assuming that the difference absorbance signal arises predominately due to state filling, we would expect the charge recombination dynamics to be homogeneous at all wavelengths, contrary to what is observed in the present case. Taken as a whole, we have thus ascribed the excited-state spectral features in $CH_3NH_3PbI_3$ to a ligand to metal charge-transfer band (reaction 4), which is seen at wavelengths shorter than 680 nm, with similar spectral features (photoinduced absorption) to an I_2 species, as discussed above. In addition, a valence to conduction band transition (reaction 5) is responsible for the 760 nm bleach (Figure 3B).[21]

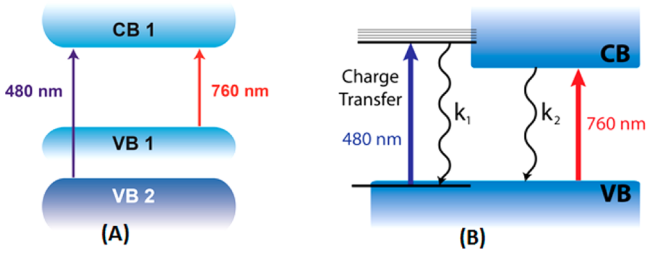

Figure 3. Schematic diagram illustrating the prevailing band structure models proposed for $CH_3NH_3PbI_3$ showing (A) the dual valence bands and (B) the coexistence of a charge-transfer band along with the semiconductor band structure. These models have been invoked to explain the photoinduced bleaches at 480 and 760 nm. Adapted from refs 21 and 23 with permission from The Royal Society of Chemistry and Nature Publishing Group.

$$CH_3NH_3PbI_3 + h\nu \rightarrow (CH_3NH_3PbI \cdots I_2) \quad (4)$$

$$CH_3NH_3PbI_3 + h\nu \rightarrow CH_3NH_3PbI_3(e + h) \quad (5)$$

Investigating the Excited State through Photoluminescence. The photoluminescence (PL) of the perovskite film offers a convenient approach to probe the excited behavior, particularly the underlying radiative recombination processes, and also map the events related to thermalization of hot electrons. As discussed later in this work, PL has also proven to be a key tool in probing the dynamics of trap-state-mediated recombination. Both $CH_3NH_3PbI_3$ and the partially chlorine-substituted mixed halide $CH_3NH_3PbI_{3-x}Cl_x$, which may contain little or no Cl in the final annealed films,[24] exhibit very broad PL peaks centered at ~1.6 eV with minimal Stokes shift. Efforts to tune the edge emission have thus far included varying the halide composition ratio (e.g., Br^-/I^-)[25] or other component substitutions[26] or tuning the crystallite dimension.[27] Herz and co-workers have probed the time-resolved PL of $CH_3NH_3PbI_{3-x}Cl_x$ with varied excitation energy. They observed a homogeneous broadening of the PL peak (fwhm = 103 meV for the PL peak versus 56 meV for the absorption onset), which they attribute to phonon coupling effects as the most likely cause.[28] Owing to the uncertainty principle, this broad emission peak could facilitate use as a gain medium in ultrafast lasing applications. The low-threshold amplified spontaneous emission of these perovskite materials further demonstrates their potential in this application.[29,30]

Chen et al. have recently observed that, even in the case of PL, free carriers play the dominant role in the recombination dynamics.[39] These authors attribute the ultrafast evolution of the PL peak seen in Figure 4 to emission from nonthermalized free carriers. It is also suggested that PL does not arise from excitonic states and can instead proceed via the interaction of uncorrelated charge carriers. This supports the growing body of evidence that excitons are rapidly dissociated at room temperature and that, under typical photovoltaic operating conditions, the recombination dynamics of $CH_3NH_3PbI_3$ are primarily governed by the interactions of free electrons and holes.[23,30−38] A more complete discussion of this topic is included in the following section. Carrier thermalization also is seen to have an interesting effect on the amplified spontaneous emission of the perovskite films, with the kinetic interplay with thermalization-limited population inversion leading to a delayed onset and oscillatory behavior in the optical gain.

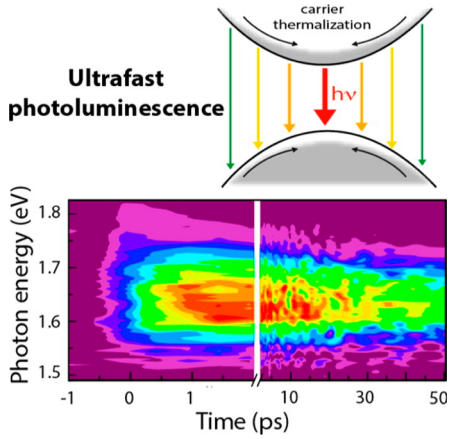

Figure 4. Ultrafast PL spectral dynamics of $CH_3NH_3PbI_{3-x}Cl_x$ after 600 nm (2.07 eV) excitation (70 $\mu J/cm^2$). Reproduced with permission from ref 39. Copyright 2015, American Chemical Society.

Spatially resolved PL measurements of $CH_3NH_3PbI_3$ nanocrystals and larger $CH_3NH_3PbI_3$ crystals have shown spatially localized PL blinking with extremely high blinking amplitude.[40] This blinking directly validates the efficient charge transport in these solution-processed films measured in other studies by indirect techniques. It also reveals the presence of very few emitting or quenching sites per crystal (one site per 10^4–10^5 nm^3), which Tian et al. associate with previously measured charge traps.[30,33] In fact, the authors suggest that the activation/deactivation of a single charge can control the PL of an entire $CH_3NH_3PbI_3$ nanocrystal.[40]

Charge Separation and Recombination. In tandem with probing the excited-state nature of the perovskite films, transient absorption spectroscopy is a convenient technique to investigate the various recombination mechanisms and their dynamics. To elucidate recombination from the band edge of $CH_3NH_3PbI_3$, perovskite films can be excited using a femtosecond laser pulse of varying intensity and the decay

DOI: 10.1021/acs.jpclett.5b00594
J. Phys. Chem. Lett. 2015, 6, 2086−2095

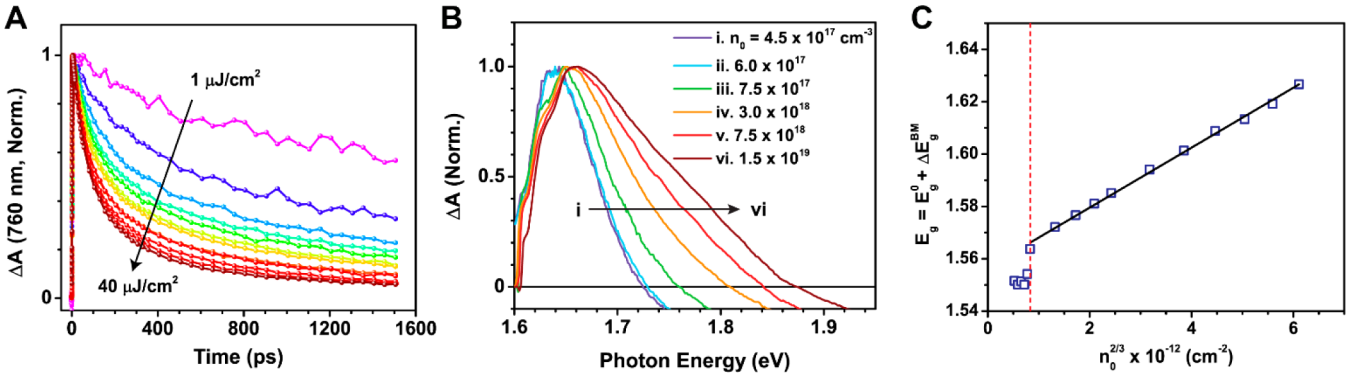

Figure 5. (A) Kinetic profiles of the 760 nm bleach recovery at various pump intensities. Higher excitation intensities result in an increased rate of band edge recombination, as indicated by the arrow. Traces are normalized to the maximum bleach signal at each excitation energy density. (B) Normalized transient absorption spectra of the band-edge transition in $CH_3NH_3PbI_3$ recorded at the maximum bleach signal (5 ps) after 387 nm pump excitation of varying intensity. The corresponding carrier densities (n_0) are indicated in the legend. (C) Modulation of the intrinsic band gap of $CH_3NH_3PbI_3$ according to the Burstein–Moss model. The vertical dashed line marks the onset of band gap broadening. The solid line is a linear fit to the data after the onset threshold. The linear trend indicates agreement with band filling by free charge carriers. Reproduced from ref 23. Copyright 2014, Nature Publishing Group.

kinetics monitored. The recovery kinetics can be modeled by the general differential rate equation shown in eq 6

$$-\frac{dn}{dt} = An + Bn^2 + Cn^3 \tag{6}$$

where n is the photogenerated charge carrier density, t is time, and A, B, and C are rate constants corresponding to trap-state-mediated recombination, nongeminate/free carrier recombination, and Auger recombination mechanisms, respectively.

The kinetic profiles of the 760 nm band edge bleach following the 387 nm laser pulse excitation are shown in Figure 5A. Fitting the recovery kinetics of the 760 nm can be adequately achieved across three orders of carrier concentrations (viz., 4.5×10^{-17}–1.5×10^{-19} cm^{-3}) by a simple second-order kinetic model, which is attributed to the recombination of free electrons and holes[23] as it is only at significantly higher charge carrier densities that Auger processes become significant.[32] The most startling aspect of this kinetic trace is the lack of any need to invoke trap-state-mediated recombination to obtain good quality fits of these kinetic decays over the time scale of several nanoseconds.[23,32] Nevertheless, although recombination through trap states is unusually slow, trap states contribute significantly to the performance of $CH_3NH_3PbI_3$ solar cells under 1 sun conditions, and recent efforts to characterize the nature of these states and control their formation are discussed in detail in the subsequent section.

A second interesting point is the atypically low second-order recombination rates observed in these films. In fact, it was seen that second-order recombination occurs up to 4 orders of magnitude slower than the rate predicted by Langevin theory, which is based on a kinetic approach to electron–hole recombination.[32] The spatial separation of electrons and holes into distinct portions of the $CH_3NH_3PbI_3$ unit cell has been predicted through density functional theory calculations and seen in experiment. Calculations have shown that the conduction band minimum is mainly composed of Pb 6p orbitals, while the valence band maximum is primarily made up of I 5p orbitals.[41,42] The I → Pb charge transfer nature of photoexcitation,[43] seen also in the work described in the previous section, leads to this spatial charge separation and the large deviation from Langevin kinetics. These factors, the combination of unexpectedly slow first-order and second-order recombination rates, make $CH_3NH_3PbI_3$ conspicuously fit for use in photovoltaics as they combine the dual advantages of low charge carrier recombination rates and high charge carrier mobilities.

Investigating the pump power dependence of the transient absorption spectra, Figure 5B reveals a distinct broadening and blue shift of the 760 nm bleach when comparing the normalized bleach signal of traces collected at increasing pump fluence. This same effect is seen in Figure 2C, in that the 760 nm band undergoes a red shift as it recovers (i.e., as the charge carrier density decreases). On the other hand, the 480 nm bleach does not exhibit any noticeable shift, maintaining a clear isosbestic point with the photoinduced absorption peak at 530 nm across the studied range of charge carrier densities.

This blue shift in the band edge bleach signal was attributed to a dynamic Burstein–Moss shift that was occurring in the perovskite films. In other words, as photogenerated carriers thermalize and accumulate at the conduction band minimum and valence band maximum, they fill sites at the band edge and, by a direct result of the Pauli exclusion principle, force higher-energy optical transitions. This behavior leads to an increase in the effective band gap of the material that is proportional to $n^{2/3}$, as shown in eq 7

$$\Delta E_g^{BM} = \frac{\hbar^2}{2m_{eh}^*}(3\pi^2 n)^{2/3} \tag{7}$$

Here n is the charge carrier density, ΔE_g^{BM} is the change in the optical band gap resulting from the Burstein–Moss band filling effect, m_{eh}^* is the reduced effective mass of electrons and holes, and $\hbar$ is the reduced Planck constant. The onset of the dynamic Burstein–Moss shift occurs at a threshold of $n = 7.5 \times 10^{17}$ cm^{-3} (Figure 5C). This correlates well with measurements of the trap state density in solution-processed $CH_3NH_3PbI_3$ films, suggesting that band filling only occurs following the accumulation of charge carriers in trap states.[29,33,44]

Key to the understanding of the excited state of $CH_3NH_3PbI_3$ films is the knowledge of whether the electron–hole pairs created upon photoexcitation exist as free carriers or excitons. Exciton binding energies have been estimated using a large number of different techniques to be

DOI: 10.1021/acs.jpclett.5b00594
J. Phys. Chem. Lett. 2015, 6, 2086–2095

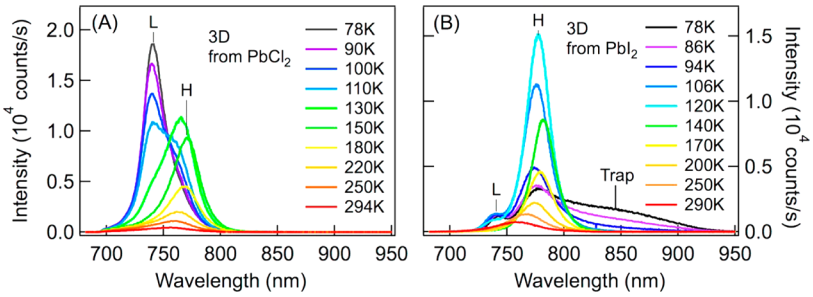

Figure 6. (A) Temperature-dependent fluorescence spectra from the low-temperature cubic phase (L) and room-temperature tetragonal phase (H) of the $CH_3NH_3PbI_3$ perovskite thin film from a $PbCl_2$ precursor and (B) that from a PbI_2 precursor. Reproduced with permission from ref 63. Copyright 2015, American Chemical Society.

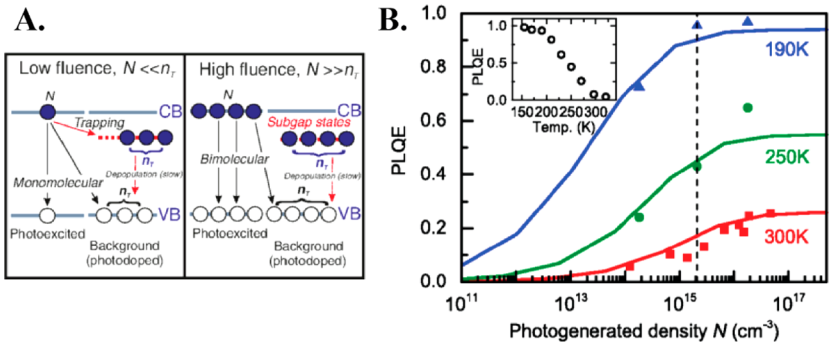

Figure 7. (A) Schematic to illustrate recombination mechanisms for the low- and high-fluence regimes. (B) PL quantum efficiency (PLQE) at varying temperatures. The inset shows PLQE as a function of temperature through the range in which the perovskite crystal remains in the tetragonal phase under quasi-steady-state excitation corresponding to $N \approx 2 \times 10^{15}$ cm^{-3}. Reproduced from ref 33 with permission from the American Physical Society.

less than 50 meV,[5,31,37,45−50] which would indicate a thermal equilibrium between excitons and free carriers at room temperature ($k_BT \approx 25$ meV). This equilibrium is determined both by the binding energy and by the excitation density, which has been estimated for $CH_3NH_3PbI_3$ to be between 10^{13} and 10^{15} cm^{-3} under steady-state solar illumination.[31] Even when using exciton binding energies at the high end of the measured range (ie. E_b = 50 meV), it has been calculated by Stranks et al. that, under operating conditions at room temperature, electron−hole pairs exist mainly as free charges, with only a fraction (≤10%) existing as excitons.[33] Recent measurements by Lin et al. have determined the real part of the static dielectric constant to be ∼70, leading to an estimated exciton binding energy of 2 meV and a strong indication of the nonexcitonic nature of $CH_3NH_3PbI_3$ films.[50] In addition, it has been suggested that exciton screening caused by the combined rotational motion of the methylammonium cations can lead to stabilization of a higher fraction of free carriers.[51]

Band filling provides experimental evidence that charges exist, at least predominately, in the perovskite as free carriers,[23] and the ultrafast disappearance of sub-band-gap-photoinduced absorption feature in the transient absorption spectrum is indicative of the disappearance of correlated charge pairs and the formation of free carriers.[30,39] Furthermore, the dynamics of the PL peak provides further evidence in support of the dominance of free carriers versus excitons,[38,39] although the Coulombic attraction of electrons and holes appears to be important.[52]

Contribution and Importance of Trap States. Somewhat surprisingly for a solution-processed material, $CH_3NH_3PbI_3$ has very high mobilities of both electrons and holes, with reported values of 6−66 cm^2 V^{-1} s^{-1}.[26,32,37,53−55] Combined with this, electron and hole diffusion lengths have been reported from 100 nm to 175 μm depending on the measurement technique and details of film fabrication.[22,37,56−59]

Theoretical investigations have suggested that these favorable properties arise due to the high proportion of shallow defect sites that form in $CH_3NH_3PbI_3$ films.[60,61] Trap state densities in typical solution-processed $CH_3NH_3PbI_3$ films appear to range between 1×10^{16} and 1×10^{17} cm^{-3},[23,29,33,44] roughly one trap site per million unit cells; however, device characterization has indicated that trap-state-mediated recombination is the dominant recombination pathway under operating conditions due to the slow recombination of free carriers.[62] On the other hand, new materials processing techniques for single $CH_3NH_3PbI_3$ crystals have demonstrated that defect densities of approximately 6 orders of magnitude lower than this are achievable, although the applicability of these techniques for devices must be more fully explored.[58,59]

The exact details of the processing conditions are critical for controlling trap formations. Zhu and co-workers clearly demonstrate this effect through low-temperature emission measurements of $CH_3NH_3PbI_3$ films formed from $PbCl_2$ (Figure 6A) and PbI_2 (Figure 6B) precursors.[63] Initially, with decreasing temperature, the primary emission band arising from charge carrier recombination becomes narrower and increases in intensity in both of these films. However, in the case of films prepared using PbI_2 as a precursor, at very low temperature (<100 K), a longer-wavelength emission (800−950 nm) arising from the trap sites becomes dominant. On the other hand, films prepared from $PbCl_2$ showed no such trap state emission. Similar control of trap states was achieved by Buin et al. when

DOI: 10.1021/acs.jpclett.5b00594
J. Phys. Chem. Lett. 2015, 6, 2086−2095

using PbI_2 and $Pb(Ac)_2$ as lead precursors.[57] In this study, it was found that iodine-deficient $CH_3NH_3PbI_3$ films formed using $Pb(Ac)_2$ yielded a factor of 3 increase in the carrier diffusion length. This improvement was attributed to the relative absence of deep traps in iodine-poor compared to iodine-rich $CH_3NH_3PbI_3$ films, and it was suggested that a similar mechanism underlies the low trap state density in films formed from $PbCl_2$.[57] These iodide-poor films also have been shown to perform superiorly in photovoltaic devices.[24] Alternatively, it may be possible to passivate undercoordinated lead at the surface by treating the $CH_3NH_3PbI_3$ films using a Lewis base.[64,65]

Because of the long lifetime of trap states in $CH_3NH_3PbI_3$, the recombination mechanism is excitation-dependent (Figure 7A). The PL of $CH_3NH_3PbI_3$ at varying photogenerated carrier density and temperature, shown in Figure 7B, shows the role that trap states play in reducing the PL quantum efficiency at low charge density.[33] Thus, decreasing trap states is clearly valuable for LEDs but also for solar cells as they seek to approach the Shockley–Quessier limit.[66] Further controlling the formation of traps and understanding their nature are of eminent importance due to their role in dictating device performance.

Further controlling the formation of traps and understanding their nature are of eminent importance due to their role in dictating device performance.

Effect of Moisture on Excited-State Properties. One of the widely debated issues of perovskite solar cells is the effect of atmospheric humidity on the photovoltaic performance. While some low level of moisture may be beneficial during the initial crystallization of perovskite films,[67,68] it becomes detrimental if unsealed cells are exposed to even relatively low levels of humidity. As shown in Figure 8, the external quantum efficiency of a prototypical perovskite solar cell substantially deteriorated in a matter of weeks when stored at 50% relative humidity (RH). Furthermore, high levels of humidity, such as 90%, led to near-total degradation in photovoltaic performance in just 4 days. One obvious question arising out of this is what are the transformations that lead to the deterioration of photovoltaic performance? It has been suggested that water could catalytically deprotonate $CH_3NH_3^+$ within the $CH_3NH_3PbI_3$ structure to form CH_3NH_2, HI, and PbI_2.[69,70]

Recent crystallographic studies have expanded on this mechanism, indicating that the initial step in the degradation is the formation of a hydrate.[18,71] Likewise, DFT calculations indicate that water molecules degrade the perovskite structure because it destabilizes the hydrogen bonding between the PbI_6 octahedra and methylamine.[72] While the structure of the hydrate formed was not conclusively determined from the initial studies,[18,71] it was proposed that it could be the dihydrate $(CH_3NH_3)_4PbI_6{\cdot}2H_2O$, which had previously been described by Vincent and co-workers as forming from solutions of $Pb(NO_3)_2$ and excess aqueous CH_3NH_3I below 40 °C.[73] However, further efforts by Leguy et al. to characterize this hydrate have revealed that it is instead the monohydrate, $CH_3NH_3PbI_3{\cdot}H_2O$, that is formed upon humidity exposure, while the dihydrate can be formed by further hydration of $CH_3NH_3PbI_3{\cdot}H_2O$, as shown in eq 8[74]

$$4CH_3NH_3PbI_3 + 4H_2O \rightleftharpoons 4[CH_3NH_3PbI_3{\cdot}H_2O] \rightleftharpoons (CH_3NH_3)_4PbI_6{\cdot}2H_2O + 3PbI_2 + 2H_2O \quad (8)$$

This intermediate monohydrate can revert back to crystalline $CH_3NH_3PbI_3$ when it is dehydrated, and initial evidence suggests that even photovoltaic performance can be restored by this dehydration.[74] On the other hand, exposure to condensed water results in the irreversible conversion to PbI_2 and, eventually, the complete dissolution of the $CH_3NH_3PbI_3$ layer.[75] Exposure of the $CH_3NH_3PbI_3$ monohydrate to light appears to also result in the irreversible decomposition to PbI_2 without the need for excess H_2O.[18,76−78]

Monitoring the ultrafast excited-state dynamics of the degrading films using femtosecond transient absorption spectroscopy reveals several salient features (Figure 9). As

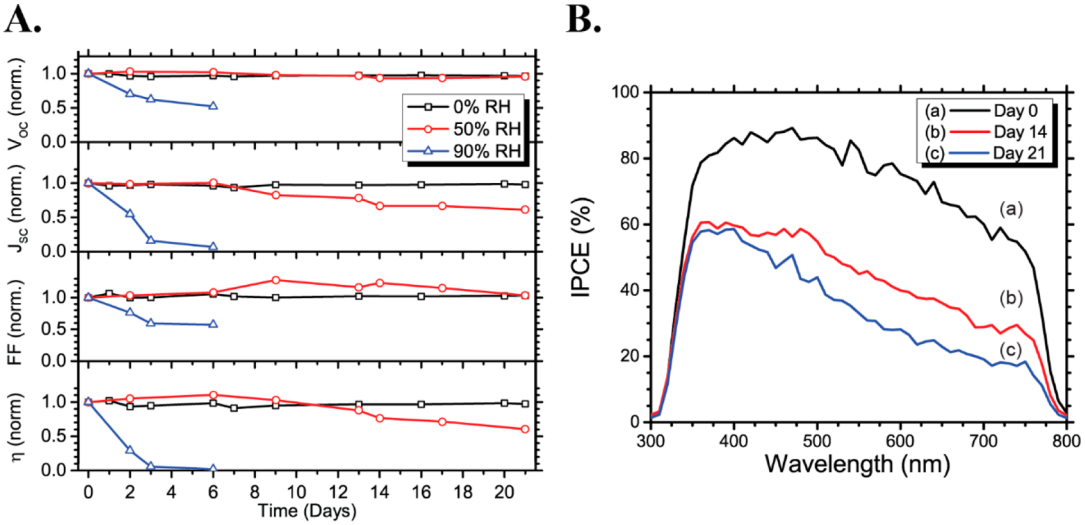

Figure 8. (A) Stacked plot of the normalized performance parameters with time for solar cells stored in 0, 50, and 90% RH. Initial efficiencies were 13.1, 10.6, and 12.1%, respectively. (B) IPCE spectra of a perovskite solar cell that was stored in 50% RH taken following exposure to these conditions for (a) 0, (b) 14, and (c) 21 days. Adapted with permission from ref 18. Copyright 2015, American Chemical Society.

DOI: 10.1021/acs.jpclett.5b00594
J. Phys. Chem. Lett. 2015, 6, 2086−2095

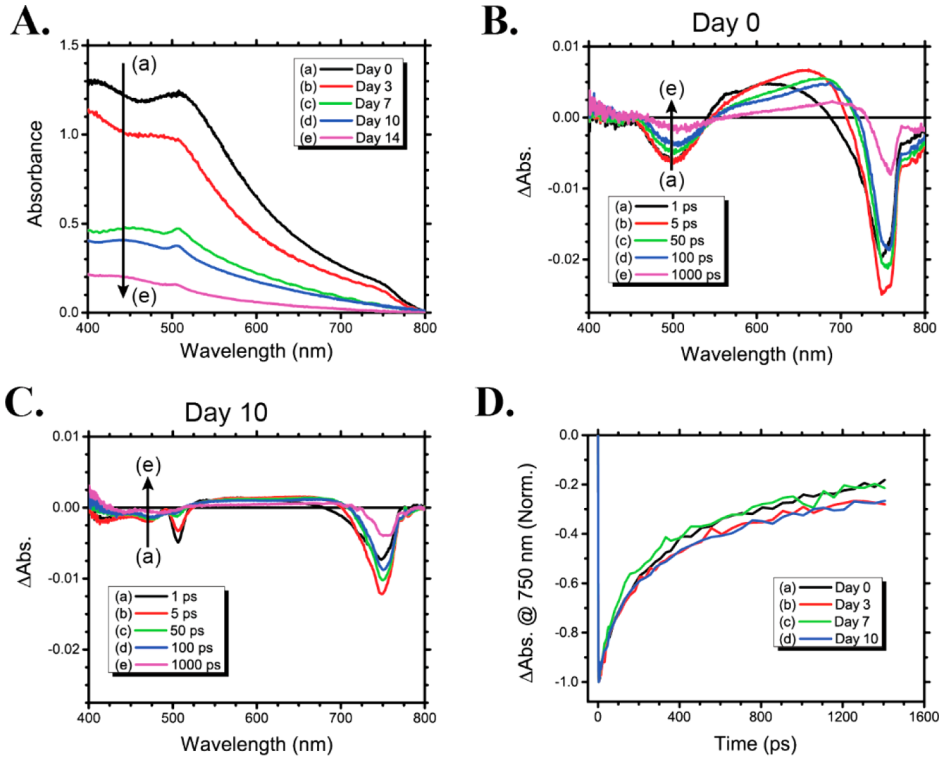

Figure 9. (A) UV−visible absorption spectra of the $CH_3NH_3PbI_3$ film stored at room temperature in the dark under 90% RH for 0−14 days. Time-resolved absorption difference spectra after (B) 0 and (C) 10 days at these conditions. (D) Time-resolved kinetic traces assembled at 750 nm over this time period. Adapted with permission from ref 18. Copyright 2015, American Chemical Society.

discussed in the previous sections, initially, the perovskite film exhibits two bleach bands and an induced absorption in the 500−650 nm region. A gradual disappearance of the characteristic perovskite spectral features in 90% RH occurs over 14 days, concomitant with appearance of a photoinduced bleach at 508 nm. This new peak is associated with crystalline PbI_2 and most likely forms upon laser excitation of the hydrated $CH_3NH_3PbI_3$.[18] The disappearance of the characteristic perovskite peaks and growth of the 508 nm bleach provide strong evidence that the high-energy bleach peak is intrinsic to $CH_3NH_3PbI_3$.

Interestingly, the decay kinetics of the perovskite films subjected to 90% RH for 10 days exhibited no significant changes in decay kinetics over the course of 1.5 ns when probed at any of the perovskite peaks (490, 625, or 750 nm). Loss of absorbance appears to occur slower than loss of photovoltaic performance, and the spectral fingerprint of $CH_3NH_3PbI_3$ is still observed even in highly degraded films.[18] This implies that the majority of performance deterioration may be due to changes in the surface and not the bulk,[18,74] although further study is required to elucidate the mechanistic details of photovoltaic performance deterioration.

Moving Forward: Tackling Future Challenges. Initial efforts to understand the excited-state behavior were earlier summarized by Sum and Mathews, providing a preliminary understanding of the photophysical mechanisms in $CH_3NH_3PbI_3$ films.[79] Given the rapid advance of the perovskite field, the present work further elaborates on this topic, providing greater detail on the mechanisms of charge separation, recombination, and trapping. This insight into the photophysical properties of $CH_3NH_3PbI_3$ will be critical to the continued progress of perovskite solar cells. However, transporting charge carriers to and into electron/hole conducting layers is an important aspect that is yet to be fully developed.[80] Most of the studies to date reflect testing of different electron and hole transport layers for their photovoltaic performance.[81] Diverse transient spectroscopic techniques will be of value in providing further insight into unraveling the multifaceted properties of the perovskite excited state. These techniques should also be useful in elucidating the fundamental mechanism behind the anomalous hysteresis seen in perovskite solar cells.[82−84] Other important scientific questions concerning perovskite solar cells were discussed during the recent Material Research Society meeting in Boston and have been clearly summarized by Hodes and co-workers.[12]

In the solution-based deposition of hybrid perovskites, these materials emerge from lead halide complexes that are formed in solution and are transformed into the three-dimensional perovskite structure upon solvent evaporation and annealing. Thus, the nature of the precursors and solvents can have a significant impact on the resultant perovskite films. Many of the semiconducting properties can be tuned through distortions of the metal halide lattice induced by the organic (or inorganic) cation.[26] Further experimental and theoretical work is required to fully characterize the nature and role of defects in the perovskite structure and better understand their correlation to photovoltaic performance. Reconciliation of these different crystallographic aspects and development of satisfactory models that take these issues into account will be an important matter for researchers to address in the near future.

Finally, the major issue pertaining to the practical application of perovskite solar cells is ambient stability, particularly stability with respect to moisture. This point is especially critical if the high photovoltage of perovskite solar cells is to be utilized for water splitting devices.[85,86] A better experimental and theoretical understanding of the surface interactions with water is critical. It is promising that experiments and

DOI: 10.1021/acs.jpclett.5b00594
J. Phys. Chem. Lett. 2015, 6, 2086−2095

calculations performed thus far point to the reversibility of the initial monohydrate, $CH_3NH_3PbI_3{\cdot}H_2O$, formed by the interaction between H_2O and $CH_3NH_3PbI_3$.[18,71−74] It has also been shown that the careful selection of appropriate hole transport materials can lead to improved device stability.[71,76,87] Further promise is seen by new hybrid perovskite materials, such as the layered hybrid perovskite $(C_6H_5(CH_2)_2NH_3)_2(CH_3NH_3)_2[Pb_3I_{10}]$,[77] which are engineered to better withstand moisture exposure. Complete details of the degradation process are still missing and sorely needed.

The major issue pertaining to the practical application of perovskite solar cells is ambient stability, particularly stability with respect to moisture.

As discussed in this Perspective, time-resolved spectroscopic techniques offer valuable information about the excited-state properties of perovskite films. Efforts are still needed to better combine these experimental studies with theoretical modeling of the excited-state behavior to develop a more complete picture of the perovskite excited state. The curious properties of $CH_3NH_3PbI_3$ and the wide range of different hybrid perovskite materials ensure that unraveling the photophysical properties of hybrid perovskite films will remain a stimulating challenge for researchers to tackle.

AUTHOR INFORMATION

Corresponding Author

*E-mail: pkamat@nd.edu. Website: www.kamatlab.com.

Notes

The authors declare no competing financial interest.

Biographies

Jeffrey A. Christians received a B.S. in Chemical Engineering and Chemistry from Calvin College in 2010 and a Ph.D. in Chemical and Biomolecular Engineering from the University of Notre Dame in 2015. He will soon be joining Joseph Luther's group as a postdoctoral researcher at the National Renewable Energy Laboratory.

Joseph S. Manser received his B.S. in Chemistry from Catawba College in 2011. He is currently a Ph.D. candidate in the Department Chemical and Biomolecular Engineering at the University of Notre Dame. His research interests include understanding the underlying material and device properties that govern the performance of next-generation photovoltaics.

Prashant V. Kamat is the Rev. John A. Zahm, C.S.C., Professor of Science at the University of Notre Dame. He earned his Ph.D. in Physical Chemistry from Bombay University in 1979 and was a postdoctoral researcher at Boston University and the University of Texas at Austin before joining Notre Dame.

ACKNOWLEDGMENTS

This work was supported by the Division of Chemical Sciences, Geosciences, and Biosciences, Office of Basic Energy Sciences of the U.S. Department of Energy through Award DE-FC02-04ER15533. J.A.C. acknowledges the Jana & Patrick Eilers Energy Research Fellowship and the Bayer Predoctoral Research Fellowship, and J.S.M. acknowledges the support of ND Energy, University of Notre Dame. This is contribution number NDRL No. 5068 from the Notre Dame Radiation Laboratory.

REFERENCES

(1) Wells, H. L. Über Die Cäsium- Und Kalium-Bleihalogenide. *Z. Anorg. Chem.* **1893**, *3* (1), 195−210.

(2) Møller, C. K. Crystal Structure and Photoconductivity of Cæsium Plumbohalides. *Nature* **1958**, *182* (4647), 1436−1436.

(3) Calabrese, J.; Jones, N. L.; Harlow, R. L.; Herron, N.; Thorn, D. L.; Wang, Y. Preparation and Characterization of Layered Lead Halide Compounds. *J. Am. Chem. Soc.* **1991**, *113* (6), 2328−2330.

(4) Mitzi, D. B.; Feild, C. A.; Harrison, W. T. A.; Guloy, A. M. Conducting Tin Halides with a Layered Organic-Based Perovskite Structure. *Nature* **1994**, *369* (6480), 467−469.

(5) Ishihara, T. Optical Properties of PbI-Based Perovskite Structures. *J. Lumin.* **1994**, *60−61*, 269−274.

(6) Papavassiliou, G. C.; Koutselas, I. B.; Terzis, A.; Whangbo, M.-H. Structural and Electronic Properties of the Natural Quantum-Well System $(C_6H_5CH_2CH_2NH_3)_2SnI_4$. *Solid State Commun.* **1994**, *91* (9), 695−698.

(7) Morimoto, S.; Tsutsui, T.; Saito, S. Electroluminescent Device Using Two Dimensional Semiconductor $(C_6H_5C_2H_4NH_3)_2PbI_4$ as an Emitter. *Synth. Met.* **1995**, *71* (1−3), 2013−2014.

(8) Hattori, T.; Taira, T.; Era, M.; Tsutsui, T.; Saito, S. Highly Efficient Electroluminescence from a Heterostructure Device Combined with Emissive Layered-Perovskite and an Electron-Transporting Organic Compound. *Chem. Phys. Lett.* **1996**, *254* (1−2), 103−108.

(9) Kojima, A.; Teshima, K.; Shirai, Y.; Miyasaka, T. Organometal Halide Perovskites as Visible-Light Sensitizers for Photovoltaic Cells. *J. Am. Chem. Soc.* **2009**, *131* (17), 6050−6051.

(10) Im, J.-H.; Lee, C.-R.; Lee, J.-W.; Park, S.-W.; Park, N.-G. 6.5% Efficient Perovskite Quantum-Dot-Sensitized Solar Cell. *Nanoscale* **2011**, *3* (10), 4088−4093.

(11) Green, M. A.; Emery, K.; Hishikawa, Y.; Warta, W.; Dunlop, E. D. Solar Cell Efficiency Tables (Version 45). *Prog. Photovoltaics Res. Appl.* **2015**, *23*, 1−9.

(12) Egger, D. A.; Edri, E.; Cahen, D.; Hodes, G. Perovskite Solar Cells: Do We Know What We Do Not Know? *J. Phys. Chem. Lett.* **2015**, 4−7.

(13) Jean, J.; Brown, P. R.; Jaffe, R. L.; Buonassisi, T.; Bulovic, V. Pathways for Solar Photovoltaics. *Energy Environ. Sci.* **2015**, *8*, 1200−1219.

(14) Stranks, S. D.; Nayak, P. K.; Zhang, W.; Stergiopoulos, T.; Snaith, H. J. Formation of Thin Films of Organic−Inorganic Perovskites for High-Efficiency Solar Cells. *Angew. Chem., Int. Ed.* **2015**, *54* (11), 3240−3248.

(15) Snaith, H. J. Perovskites: The Emergence of a New Era for Low-Cost, High-Efficiency Solar Cells. *J. Phys. Chem. Lett.* **2013**, *4* (21), 3623−3630.

(16) Park, N. Organo-Metal Perovskite Light Absorbers toward 20% Efficiency Low-Cost Solid-State Mesoscopic Solar Cell. *J. Phys. Chem. Lett.* **2013**, *4* (15), 2423−2429.

(17) Gao, P.; Grätzel, M.; Nazeeruddin, M. K. Organohalide Lead Perovskites for Photovoltaic Applications. *Energy Environ. Sci.* **2014**, *7*, 2448−2463.

(18) Christians, J. A.; Miranda Herrera, P. A.; Kamat, P. V. Transformation of the Excited State and Photovoltaic Efficiency of $CH_3NH_3PbI_3$ Perovskite upon Controlled Exposure to Humidified Air. *J. Am. Chem. Soc.* **2015**, *137* (4), 1530−1538.

(19) Williams, S. T.; Zuo, F.; Chueh, C.; Liao, C.; Liang, P.; Jen, A. K.-Y. Role of Chloride in the Morphological Evolution of Organo-Lead Halide Perovskite Thin Films. *ACS Nano* **2014**, *8* (10), 10640−10654.

(20) Horváth, O.; Mikó, I. Spectra, Equilibrium and Photoredox Chemistry of Iodobismuthate(III) Complexes in Acetonitrile. *Inorg. Chim. Acta* **2000**, *304*, 210−218.

DOI: 10.1021/acs.jpclett.5b00594
J. Phys. Chem. Lett. 2015, 6, 2086−2095

(21) Stamplecoskie, K. G.; Manser, J. S.; Kamat, P. V. Dual Nature of the Excited State in Organic−Inorganic Lead Halide Perovskites. *Energy Environ. Sci.* **2015**, *8*, 208−215.
(22) Xing, G.; Mathews, N.; Sun, S.; Lim, S. S.; Lam, Y. M.; Gratzel, M.; Mhaisalkar, S.; Sum, T. C. Long-Range Balanced Electron- and Hole-Transport Lengths in Organic−Inorganic $CH_3NH_3PbI_3$. *Science* **2013**, *342* (6156), 344−347.
(23) Manser, J. S.; Kamat, P. V. Band Filling with Free Charge Carriers in Organometal Halide Perovskites. *Nat. Photonics* **2014**, *8*, 737−743.
(24) Zhang, W.; Saliba, M.; Moore, D. T.; Pathak, S.; Horantner, M.; Stergiopoulos, T.; Stranks, S. D.; Eperon, G. E.; Alexander-Webber, J. A.; Abate, A.; et al. Ultrasmooth Organic−Inorganic Perovskite Thin-Film Formation and Crystallization for Efficient Planar Heterojunction Solar Cells. *Nat. Commun.* **2014**, *6*, 6142.
(25) Zhang, M.; Yu, H.; Lyu, M.; Wang, Q.; Yun, J.-H.; Wang, L. Composition-Dependent Photoluminescence Intensity and Prolonged Recombination Lifetime of Perovskite $CH_3NH_3PbBr_{3-x}Cl_x$ Films. *Chem. Commun. (Cambridge)* **2014**, *3* (100), 1−4.
(26) Stoumpos, C. C.; Malliakas, C. D.; Kanatzidis, M. G. Semiconducting Tin and Lead Iodide Perovskites with Organic Cations: Phase Transitions, High Mobilities, and Near-Infrared Photoluminescent Properties. *Inorg. Chem.* **2013**, *52* (15), 9019−9038.
(27) D'Innocenzo, V.; Srimath Kandada, A. R.; De Bastiani, M.; Gandini, M.; Petrozza, A. Tuning the Light Emission Properties by Band Gap Engineering in Hybrid Lead-Halide Perovskite. *J. Am. Chem. Soc.* **2014**, *136*, 17730−17733.
(28) Wehrenfennig, C.; Liu, M.; Snaith, H. J.; Johnston, M. B.; Herz, L. M. Homogeneous Emission Line Broadening in the Organo Lead Halide Perovskite $CH_3NH_3PbI_{3-x}Cl_x$. *J. Phys. Chem. Lett.* **2014**, *5*, 1300−1306.
(29) Xing, G.; Mathews, N.; Lim, S. S.; Yantara, N.; Liu, X.; Sabba, D.; Grätzel, M.; Mhaisalkar, S.; Sum, T. C. Low-Temperature Solution-Processed Wavelength-Tunable Perovskites for Lasing. *Nat. Mater.* **2014**, *13* (March), 476−480.
(30) Deschler, F.; Price, M.; Pathak, S.; Klintberg, L. E.; Jarausch, D. D.; Higler, R.; Hüttner, S.; Leijtens, T.; Stranks, S. D.; Snaith, H. J.; et al. High Photoluminescence Efficiency and Optically Pumped Lasing in Solution-Processed Mixed Halide Perovskite Semiconductors. *J. Phys. Chem. Lett.* **2014**, *5*, 1421−1426.
(31) D'Innocenzo, V.; Grancini, G.; Alcocer, M. J. P.; Kandada, A. R. S.; Stranks, S. D.; Lee, M. M.; Lanzani, G.; Snaith, H. J.; Petrozza, A. Excitons versus Free Charges in Organo-Lead Tri-Halide Perovskites. *Nat. Commun.* **2014**, *5*, 3586.
(32) Wehrenfennig, C.; Eperon, G. E.; Johnston, M. B.; Snaith, H. J.; Herz, L. M. High Charge Carrier Mobilities and Lifetimes in Organolead Trihalide Perovskites. *Adv. Mater.* **2014**, *26* (10), 1584−1589.
(33) Stranks, S. D.; Burlakov, V. M.; Leijtens, T.; Ball, J. M.; Goriely, A.; Snaith, H. J. Recombination Kinetics in Organic−Inorganic Perovskites: Excitons, Free Charge, and Subgap States. *Phys. Rev. Appl.* **2014**, *034007*, 1−8.
(34) You, J.; Hong, Z.; Yang, Y. M.; Chen, Q.; Cai, M.; Song, T.; Chen, C.; Lu, S.; Liu, Y.; Zhou, H.; et al. Low-Temperature Solution-Processed Perovskite Solar Cells with High Efficiency and Flexibility. *ACS Nano* **2014**, *8* (2), 1674−1680.
(35) Edri, E.; Kirmayer, S.; Mukhopadhyay, S.; Gartsman, K.; Hodes, G.; Cahen, D. Elucidating the Charge Carrier Separation and Working Mechanism of $CH_3NH_3PbI_{(3-x)}Cl_x$ Perovskite Solar Cells. *Nat. Commun.* **2014**, *5*, 3461.
(36) Zhang, W.; Saliba, M.; Stranks, S. D.; Sun, Y.; Shi, X.; Wiesner, U.; Snaith, H. J. Enhancement of Perovskite-Based Solar Cells Employing Core−Shell Metal Nanoparticles. *Nano Lett.* **2013**, *13* (9), 4505−4510.
(37) Savenije, T. J.; Ponseca, C. S.; Kunneman, L.; Abdellah, M.; Zheng, K.; Tian, Y.; Zhu, Q.; Canton, S. E.; Scheblykin, I. G.; Pullerits, T.; et al. Thermally Activated Exciton Dissociation and Recombination Control the Carrier Dynamics in Organometal Halide Perovskite. *J. Phys. Chem. Lett.* **2014**, *5*, 2189−2194.
(38) Yamada, Y.; Nakamura, T.; Endo, M.; Wakamiya, A.; Kanemitsu, Y. Photocarrier Recombination Dynamics in Perovskite $CH_3NH_3PbI_3$ for Solar Cell Applications. *J. Am. Chem. Soc.* **2014**, *136* (33), 11610−11613.
(39) Chen, K.; Barker, A. J.; Morgan, F. L. C.; Halpert, J. E.; Hodgkiss, J. M. Effect of Carrier Thermalization Dynamics on Light Emission and Amplification in Organometal Halide Perovskites. *J. Phys. Chem. Lett.* **2015**, *6*, 153−158.
(40) Tian, Y.; Merdasa, A.; Peter, M.; Abdellah, M.; Zheng, K.; Ponseca, C. S.; Pullerits, T.; Yartsev, A.; Sundström, V.; Scheblykin, I. G. Giant Photoluminescence Blinking of Perovskite Nanocrystals Reveals Single-Trap Control of Luminescence. *Nano Lett.* **2015**, *15*, 1603−1608.
(41) Baikie, T.; Fang, Y.; Kadro, J. M.; Schreyer, M.; Wei, F.; Mhaisalkar, S. G.; Gratzel, M.; White, T. J. Synthesis and Crystal Chemistry of the Hybrid Perovskite $(CH_3NH_3)PbI_3$ for Solid-State Sensitised Solar Cell Applications. *J. Mater. Chem. A* **2013**, *1*, 5628.
(42) Umebayashi, T.; Asai, K.; Kondo, T.; Nakao, A. Electronic Structures of Lead Iodide Based Low-Dimensional Crystals. *Phys. Rev. B* **2003**, *67*, 2−7.
(43) Gottesman, R.; Haltzi, E.; Gouda, L.; Tirosh, S.; Bouhadana, Y.; Zaban, A.; Mosconi, E.; De Angelis, F. Extremely Slow Photoconductivity Response of $CH_3NH_3PbI_3$ Perovskites Suggesting Structural Changes under Working Conditions. *J. Phys. Chem. Lett.* **2014**, *5* (15), 2662−2669.
(44) Samiee, M.; Konduri, S.; Ganapathy, B.; Kottokkaran, R.; Abbas, H. A.; Kitahara, A.; Joshi, P.; Zhang, L.; Noack, M.; Dalal, V. Defect Density and Dielectric Constant in Perovskite Solar Cells. *Appl. Phys. Lett.* **2014**, *105*, 153502.
(45) Tanaka, K.; Takahashi, T.; Ban, T.; Kondo, T.; Uchida, K.; Miura, N. Comparative Study on the Excitons in Lead-Halide-Based Perovskite-Type Crystals $CH_3NH_3PbBr_3$ $CH_3NH_3PbI_3$. *Solid State Commun.* **2003**, *127* (9−10), 619−623.
(46) Hirasawa, M.; Ishihara, T.; Goto, T.; Uchida, K.; Miura, N. Magnetoabsorption of the Lowest Exciton in Perovskite-Type Compound $(CH_3NH_3)PbI_3$. *Phys. B: Condens. Matter* **1994**, *201*, 427−430.
(47) Sun, S.; Salim, T.; Mathews, N.; Duchamp, M.; Boothroyd, C.; Xing, G.; Sum, T. C.; Lam, Y. M. The Origin of High Efficiency in Low-Temperature Solution-Processable Bilayer Organometal Halide Hybrid Solar Cells. *Energy Environ. Sci.* **2014**, *7*, 399.
(48) Papavassiliou, G. C.; Mousdis, G. A.; Koutselas, I. B. Excitonic Bands in the Spectra of Some Organic−Inorganic Hybrid Compounds Based on Metal Halide Units. *Synth. Met.* **2001**, *121* (1), 1339−1340.
(49) Koutselas, I. B.; Ducasse, L.; Papavassiliou, G. C. Electronic Properties of Three- and Low-Dimensional Semiconducting Materials with Pb Halide and Sn Halide Units. *J. Phys.: Condens. Matter* **1996**, *8*, 1217−1227.
(50) Lin, Q.; Armin, A.; Chandra, R.; Nagiri, R.; Burn, P. L.; Meredith, P. Electro-Optics of Perovskite Solar Cells. *Nat. Photonics* **2014**, *9* (2), 106−112.
(51) Even, J.; Pedesseau, L.; Katan, C. Analysis of Multivalley and Multibandgap Absorption and Enhancement of Free Carriers Related to Exciton Screening in Hybrid Perovskites. *J. Phys. Chem. C* **2014**, *118*, 11566−11572.
(52) Saba, M.; Cadelano, M.; Marongiu, D.; Chen, F.; Sarritzu, V.; Sestu, N.; Figus, C.; Aresti, M.; Piras, R.; Geddo Lehmann, A.; et al. Correlated Electron−hole Plasma in Organometal Perovskites. *Nat. Commun.* **2014**, *5* (May), 5049.
(53) Leijtens, T.; Stranks, S. D.; Eperon, G. E.; Lindblad, R.; Johansson, E. M. J.; McPherson, I. J.; Rensmo, H.; Ball, J. M.; Lee, M. M.; Snaith, H. J. Electronic Properties of Meso-Superstructured and Planar Organometal Halide Perovskite Films: Charge Trapping, Photodoping, and Carrier Mobility. *ACS Nano* **2014**, *8* (7), 7147−7155.
(54) Nie, W.; Tsai, H.; Asadpour, R.; Blancon, J.-C.; Neukirch, A. J.; Gupta, G.; Crochet, J. J.; Chhowalla, M.; Tretiak, S.; Alam, M. A.; et al. High-Efficiency Solution-Processed Perovskite Solar Cells with Millimeter-Scale Grains. *Science* **2015**, *347* (6221), 522−525.

DOI: 10.1021/acs.jpclett.5b00594
J. Phys. Chem. Lett. 2015, 6, 2086−2095

(55) Ponseca, C. S.; Savenije, T. J.; Abdellah, M.; Zheng, K.; Yartsev, A.; Pascher, T.; Harlang, T.; Chabera, P.; Pullerits, T.; Stepanov, A.; et al. Organometal Halide Perovskite Solar Cell Materials Rationalized: Ultrafast Charge Generation, High and Microsecond-Long Balanced Mobilities, and Slow Recombination. *J. Am. Chem. Soc.* **2014**, *136* (14), 5189−5192.
(56) Stranks, S. D.; Eperon, G. E.; Grancini, G.; Menelaou, C.; Alcocer, M. J. P.; Leijtens, T.; Herz, L. M.; Petrozza, A.; Snaith, H. J. Electron−Hole Diffusion Lengths Exceeding 1 Micrometer in an Organometal Trihalide Perovskite Absorber. *Science* **2013**, *342* (6156), 341−344.
(57) Buin, A.; Pietsch, P.; Xu, J.; Voznyy, O.; Ip, A. H.; Comin, R.; Sargent, E. H. Materials Processing Routes to Trap-Free Halide Perovskites. *Nano Lett.* **2014**, *14* (11), 6281−6286.
(58) Shi, D.; Adinolfi, V.; Comin, R.; Yuan, M.; Alarousu, E.; Buin, A.; Chen, Y.; Hoogland, S.; Rothenberger, A.; Katsiev, K.; et al. Low Trap-State Density and Long Carrier Diffusion in Organolead Trihalide Perovskite Single Crystals. *Science* **2015**, *347*, 519−522.
(59) Dong, Q.; Fang, Y.; Shao, Y.; Mulligan, P.; Qiu, J.; Cao, L.; Huang, J. Electron−Hole Diffusion Lengths > 175 μm in Solution Grown $CH_3NH_3PbI_3$ Single Crystals. *Science* **2015**, *347*, 967−970.
(60) Yin, W.-J.; Shi, T.; Yan, Y. Unusual Defect Physics in $CH_3NH_3PbI_3$ Perovskite Solar Cell Absorber. *Appl. Phys. Lett.* **2014**, *104* (6), 063903.
(61) Kim, J.; Lee, S. H.; Lee, J. H.; Hong, K. H. The Role of Intrinsic Defects in Methylammonium Lead Iodide Perovskite. *J. Phys. Chem. Lett.* **2014**, *5* (8), 1312−1317.
(62) Wetzelaer, G. A. H.; Scheepers, M.; Sempere, A. M.; Momblona, C. Trap-Assisted Non-Radiative Recombination in Organic−Inorganic Perovskite Solar Cells. *Adv. Mater.* **2015**, *27* (11), 1837−1841.
(63) Wu, X.; Trinh, M. T.; Niesner, D.; Zhu, H.; Norman, Z.; Owen, J. S.; Yaffe, O.; Kudisch, B. J.; Zhu, X.-Y. Trap States in Lead Iodide Perovskites. *J. Am. Chem. Soc.* **2015**, *137* (5), 2089−2096.
(64) Noel, N. K.; Abate, A.; Stranks, S. D.; Parrott, E. S.; Burlakov, V. M.; Goriely, A.; Snaith, H. J. Enhanced Photoluminescence and Solar Cell Performance via Lewis Base Passivation of Organic−Inorganic Lead Halide Perovskites. *ACS Nano* **2014**, *8* (10), 9815−9821.
(65) Shkrob, I. A.; Marin, T. W. Charge Trapping in Photovoltaically Active Perovskites and Related Halogenoplumbate Compounds. *J. Phys. Chem. Lett.* **2014**, *5*, 1066−1071.
(66) Shockley, W.; Queisser, H. J. Detailed Balance Limit of Efficiency of *p*−*n* Junction Solar Cells. *J. Appl. Phys.* **1961**, *32* (1961), 510−519.
(67) Bass, K. K.; McAnally, R. E.; Zhou, S.; Djurovich, P. I.; Thompson, M.; Melot, B. Influence of Moisture on the Preparation, Crystal Structure, and Photophysical Properties of Organohalide Perovskites. *Chem. Commun.* **2014**, *50*, 15819−15822.
(68) Zhou, H.; Chen, Q.; Li, G.; Luo, S.; Song, T.-B.; Duan, H.-S.; Hong, Z.; You, J.; Liu, Y.; Yang, Y. Interface Engineering of Highly Efficient Perovskite Solar Cells. *Science* **2014**, *345* (6196), 542−546.
(69) Niu, G.; Li, W.; Meng, F.; Wang, L.; Dong, H.; Qiu, Y. Study on the Stability of $CH_3NH_3PbI_3$ Films and the Effect of Post-Modification by Aluminum Oxide in All-Solid-State Hybrid Solar Cells. *J. Mater. Chem. A* **2014**, *2*, 705.
(70) Frost, J. M.; Butler, K. T.; Brivio, F.; Hendon, C. H.; Van Schilfgaarde, M.; Walsh, A. Atomistic Origins of High-Performance in Hybrid Halide Perovskite Solar Cells. *Nano Lett.* **2014**, *14* (5), 2584−2590.
(71) Yang, J.; Siempelkamp, B. D.; Liu, D.; Kelly, T. L. An Investigation of $CH_3NH_3PbI_3$ Degradation Rates and Mechanisms in Controlled Humidity Environments Using in Situ Techniques. *ACS Nano* **2015**, *9* (2), 1955−1963.
(72) Dong, X.; Fang, X.; Lv, M.; Lin, B.; Zhang, S.; Ding, J.; Yuan, N. Improvement of the Humidity Stability of Organic−Inorganic Perovskite Solar Cells Using Ultrathin Al_2O_3 Layers Prepared by Atomic Layer Deposition. *J. Mater. Chem. A* **2015**, *3*, 5360−5367.
(73) Vincent, B. R.; Robertson, K. N.; Cameron, T. S.; Knop, O. Alkylammonium Lead Halides. Part 1. Isolated PbI_6^{4-} Ions in $(CH_3NH_3)_4PbI_6{\cdot}2H_2O$. *Can. J. Chem.* **1987**, *65* (5), 1042−1046.
(74) Leguy, A.; Hu, Y.; Campoy-Quiles, M.; Alonso, M. I.; Weber, O. J.; Azarhoosh, P.; van Schilfgaarde, M.; Weller, M. T.; Bein, T.; Nelson, J.; et al. The Reversible Hydration of $CH_3NH_3PbI_3$ in Films, Single Crystals and Solar Cells. *Chem. Mater.* **2015**, DOI: 10.1021/acs.chemmater.5b00660.
(75) Hailegnaw, B.; Kirmayer, S.; Edri, E.; Hodes, G.; Cahen, D. Rain on Methylammonium Lead Iodide Based Perovskites: Possible Environmental Effects of Perovskite Solar Cells. *J. Phys. Chem. Lett.* **2015**, *6*, 1543−1547.
(76) Habisreutinger, S. N.; Leijtens, T.; Eperon, G. E.; Stranks, S. D.; Nicholas, R. J.; Snaith, H. J. Carbon Nanotube/Polymer Composite as a Highly Stable Charge Collection Layer in Perovskite Solar Cells. *Nano Lett.* **2014**, *14* (10), 5561−5568.
(77) Smith, I. C.; Hoke, E. T.; Solis-Ibarra, D.; McGehee, M. D.; Karunadasa, H. I. A Layered Hybrid Perovskite Solar-Cell Absorber with Enhanced Moisture Stability. *Angew. Chem.* **2014**, *126* (42), 11414−11417.
(78) Dualeh, A.; Tétreault, N.; Moehl, T.; Gao, P.; Nazeeruddin, M. K.; Grätzel, M. Effect of Annealing Temperature on Film Morphology of Organic−Inorganic Hybrid Pervoskite Solid-State Solar Cells. *Adv. Funct. Mater.* **2014**, *24* (21), 3250−3258.
(79) Sum, T. C.; Mathews, N. Advancements in Perovskite Solar Cells: Photophysics behind the Photovoltaics. *Energy Environ. Sci.* **2014**, 2518−2534.
(80) Marchioro, A.; Teuscher, J.; Friedrich, D.; Kunst, M.; van de Krol, R.; Moehl, T.; Grätzel, M.; Moser, J.-E. Unravelling the Mechanism of Photoinduced Charge Transfer Processes in Lead Iodide Perovskite Solar Cells. *Nat. Photonics* **2014**, *8*, 250−255.
(81) Chueh, C.-C.; Li, C.-Z.; Jen, A. K.-Y. Recent Progress and Perspective in Solution-Processed Interfacial Materials for Efficient and Stable Polymer and Organometal Perovskite Solar Cells. *Energy Environ. Sci.* **2015**, *00*, 1−30.
(82) Snaith, H. J.; Abate, A.; Ball, J. M.; Eperon, G. E.; Leijtens, T.; Noel, N. K.; Stranks, S. D.; Wang, J. T.-W.; Wojciechowski, K.; Zhang, W. Anomalous Hysteresis in Perovskite Solar Cells. *J. Phys. Chem. Lett.* **2014**, *5* (9), 1511−1515.
(83) Christians, J. A.; Manser, J. S.; Kamat, P. V. Best Practices in Perovskite Solar Cell Efficiency Measurements. Avoiding the Error of Making Bad Cells Look Good. *J. Phys. Chem. Lett.* **2015**, *6*, 852−857.
(84) Kim, H. S.; Park, N. Parameters Affecting *I*−*V* Hysteresis of $CH_3NH_3PbI_3$ Perovskite Solar Cells: Effects of Perovskite Crystal Size and Mesoporous TiO_2 Layer. *J. Phys. Chem. Lett.* **2014**, *5*, 2927−2934.
(85) Chen, Y.-S.; Manser, J. S.; Kamat, P. V. All Solution-Processed Lead Halide Perovskite-$BiVO_4$ Tandem Assembly for Photolytic Solar Fuels Production. *J. Am. Chem. Soc.* **2015**, *137* (2), 974−981.
(86) Luo, J.; Im, J.-H.; Mayer, M. T.; Schreier, M.; Nazeeruddin, M. K.; Park, N.-G.; Tilley, S. D.; Fan, H. J.; Gratzel, M. Water Photolysis at 12.3% Efficiency via Perovskite Photovoltaics and Earth-Abundant Catalysts. *Science* **2014**, *345* (6204), 1593−1596.
(87) Christians, J. A.; Fung, R. C. M.; Kamat, P. V. An Inorganic Hole Conductor for Organo-Lead Halide Perovskite Solar Cells. Improved Hole Conductivity with Copper Iodide. *J. Am. Chem. Soc.* **2014**, *136* (2), 758−764.

DOI: 10.1021/acs.jpclett.5b00594
J. Phys. Chem. Lett. 2015, 6, 2086−2095